KeAi

CHINESE ROOTS
GLOBAL IMPACT

Contents lists available at ScienceDirect

Petroleum Science

journal homepage: www.keaipublishing.com/en/journals/petroleum-science



Original Paper

Modeling of the mechano-electrochemical effect at corrosion defect with varied inclinations on oil/gas pipelines



Zhu-Wu Zhang a, b, *, Jin-Chang Wang a, Jiu-Hong Zhang a, Y. Frank Cheng b, **

- ^a College of Chemical Engineering, Fuzhou University, Fuzhou, 350116, Fujian, China
- b Department of Mechanical Engineering, University of Calgary, Calgary, T2N 1N4, Alberta, Canada

ARTICLE INFO

Article history: Received 1 May 2020 Accepted 9 November 2020 Available online 1 September 2021

Edited by Xiu-Oiu Peng

Keywords:
Pipelines
Corrosion defect assessment
Mechano-electrochemical effect
Finite element model

ABSTRACT

A 3-dimensional finite element model was built to determine the effect of inclination angle of a corrosion defect on local mechano-electrochemical (M-E) effect in a simulated soil solution. Because of the high effect of the defect inclination angle on the M-E effect, when the inclination angle is 0° (i.e., the primary axis of the defect parallel to the longitudinal direction of the pipe), the greatest stress concentration level at the defect can be observed, which is associated with the lowest corrosion potential, the greatest anodic current density and the most serious accelerated localized corrosion. When the inclination angle is 90° , the stress concentration level reduces and the corrosion potential becomes less negative, accompanying with the decreased anodic/cathodic current densities. Besides, when the ratio (r_{ca}) of the primary axial length of the defect to its secondary axial length is 1, the defect inclination does not affect the stress and the electrochemical corrosion rate at the defect. With the increase of r_{ca} , the effect of the defect inclination angle is more apparent.

© 2021 The Authors. Publishing services by Elsevier B.V. on behalf of KeAi Communications Co. Ltd. This is an open access article under the CC BY-NC-ND license (http://creativecommons.org/licenses/by-nc-nd/4.0/).

1. Introduction

External corrosion of underground oil/gas pipelines are affected by many factors including soil, moisture content, dissolved oxygen, stray current, microorganism, etc. (Yajima et al., 2015; Dai et al., 2018; Xu and Cheng 2012a, 2013; Xu et al., 2013; Qian and Cheng, 2017; Liu and Cheng 2017, 2018; Lu et al., 2018). Particularly, the pipeline corrosion is accelerated by the stressing condition through a so-called mechano-electrochemical (M-E) effect principle (Gutman, 1998; Xu and Cheng, 2012b, 2017; Sun and Cheng, 2019; Zhang et al., 2020). Generally, the localized corrosion rate at the defect on pipelines would be accelerated by the local stress concentration at the defect. At the same time, the ratio of the depth of the defect to its width is increased by enhanced corrosion reaction, which further raises the stress concentration level, as investigated in previous work conducted in the authors' group and others (Shuai et al., 2017; Sun and Cheng, 2018; Wang et al., 2018; Xu and Cheng

E-mail addresses: zwzhang@fzu.edu.cn (Z.-W. Zhang), fcheng@ucalgary.ca (Y.F. Cheng).

2013, 2017; Fatoba et al., 2018; Wang and Han, 2013). Therefore, a self-accelerating process occurring at the corrosion defect owing to the M-E effect usually causes rapid perforation of the pipeline.

For assessing the risk of pipelines containing corrosion defects, the defect shape is generally treated as semi-ellipsoid (Rajabipour and Melchers, 2013; Xie and Tian, 2018; Yi et al., 2012), where the stress distribution depends on the depth and the axial lengths of defects (Huang et al., 2014; Noda and Hayashida, 2000). For an ellipsoidal corrosion defect, its axial dimension is either perpendicular or parallel to the longitudinal direction of the pipeline. Thus, the stress distribution at the defect is symmetric relative to axes. However, the actual corrosion defect generated on a pipeline is never an ideal semi-ellipsoid (Kim and Park, 2017). In reality, the orientation of the defect can be random inclinations on pipelines. This can cause the dependence of the local stress distribution of the defect on the defect's inclination angle (θ), thus affecting the local corrosion reaction under the M-E interaction. To authors' best knowledge, the uniqueness and innovation of this work is, at the first time of its kind, to quantitatively define the local stress concentration level, corrosion potential (E_{corr}) and anodic/cathodic current densities (i_a/i_c) at defect with various inclinations on pipelines. The modeling results improve the accuracy of defect assessment on pipelines, contributing to enhanced pipeline

^{*} Corresponding author. College of Chemical Engineering, Fuzhou University, Fuzhou, 350116, Fujian, China.

^{**} Corresponding author.

integrity management.

A 3D finite element (FE) based model was built to determine the effect of the defect inclination on the local mechanoelectrochemical interaction in a near-neutral pH solution (i.e., NS4 solution) simulating the electrolyte trapped under disbonded polyethylene coating on buried pipelines (Xu and Cheng 2012a, 2013). It is noted that NS4 solution is not a soil solution. Its solution chemistry is related to soil chemistry, coating property, cathodic protection current shielding, etc. The local stress concentration level, E_{COTT} , i_{a} and i_{c} at the defect were modeled and determined to assess the local M-E effect while the pipe was under internal pressure. The effect of the defect inclination angle relative to the longitudinal direction of the pipe was analyzed, and the implication on the pipeline integrity was discussed.

2. Numerical modeling

2.1. Electrochemical corrosion model

Fig. 1a shows the FE model developed by COMSOL Multiphysics software for an \times 100 steel pipe with a semi-ellipsoidal defect exposed to the near-neutral pH solution with a pH of 6.8 (Xu and Cheng 2012a, 2013). The wall thickness (B), the outer diameter (D) and the length (L) of the pipe are 16 mm, 914.4 mm and 2000 mm, respectively, where the length (L) is enough to avoid the boundary condition effect according to the 4.9 $(DB/2)^{1/2}$ criterion (Chouchaoui and Pick, 1996), i.e., 419.1 mm from the D and B values in this work. It is the corrosion defect, rather than the whole pipe segment, that is exposed to NS4 solution. Corrosion happens mainly at the defect, but other pipe segments are coated to prevent from corrosion attack. Thus, a galvanic effect between the defect and other areas of the pipe does not occur. As a result, galvanic corrosion is not included.

The depth (b) of the semi-ellipsoidal defect was 8 mm in y-axis direction, and the half-lengths of the primary axis (i.e., c) and the secondary axis (i.e., a) were 32 mm and 8 mm, respectively. The axial ratio of the defect length ($r_{\rm ca}=c/a$), was equal to 4. The angle θ , as labeled in Fig. 1a, was the included angle between c and the z-axis, which was used to determine the orientation of the corrosion defect. When c was parallel or perpendicular to the z-axis, θ was 0° or 90°, respectively. The θ degrees modeled in this work included 0°, 15°, 30°, 45°, 60°, 75° and 90°.

According to ASME B31.4 (ASME B31.4 2009), the buried pipelines can be treated as a restrained pipe. The constraint conditions at both pipe ends were thus set as zero displacement in the longitudinal direction, but free in the radial direction. Thus, hoop stress (σ_H) and longitudinal stress (σ_L) were written as:

$$\sigma_{\rm H} = PD/2B \tag{1}$$

$$\sigma_{L} = \sigma_{E} + \nu \sigma_{H} + \frac{M}{Z} + \frac{F_{a}}{A} \tag{2}$$

where P is internal pressure, $\sigma_{\rm E}$, M and $F_{\rm a}$ are thermal expansion stress, bending moment and axial force, respectively, which were all equal to 0 in this work. ν is Poisson's ratio, Z is sectional modulus, and A is cross-sectional area. The $\sigma_{\rm L}$ can be calculated as:

$$\sigma_{\rm L} = \nu \sigma_{\rm H}$$
 (3)

A free tetrahedral mesh was used in COMSOL. Fig. 2 shows the distribution of meshes of a pipe with a defect, where the element size of the defect is smaller than other parts of the pipe in order to obtain sufficient accuracy with a reasonable computational time. Besides, the maximum von Mises stress (σ_{Mises}) at defect (θ is 0° and internal pressure is 20 MPa) tends to be stable with increased number of the elements (Fig. 3). Although the change in maximum σ_{Mises} is slight when the element size is smaller than 2 mm, the element size of 0.5 mm was selected for improved accuracy in modeling.

Fig. 1b shows the boundary condition for electrochemical corrosion occurring at the defect under disbonded coating. In

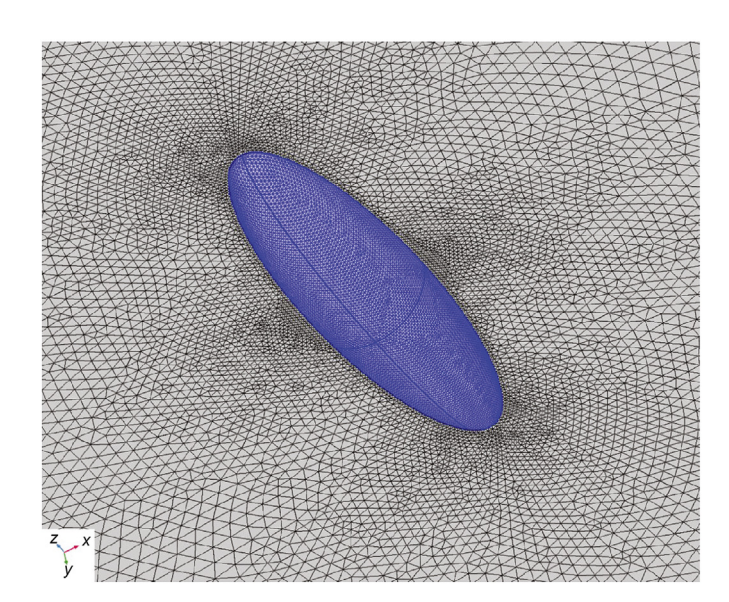


Fig. 2. Mesh distribution of the pipe segment containing a semi-ellipsoidal corrosion defect.

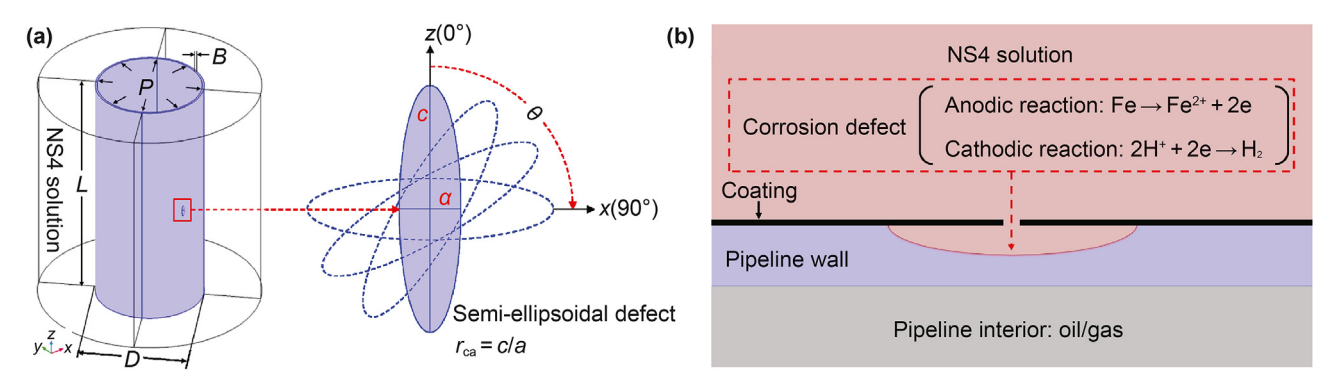


Fig. 1. (a) Schematic diagram of a 3D FE model for a pipe segment containing a semi-ellipsoidal defect exposed to NS4 solution. (b) Schematic diagram of the boundary condition for electrochemical corrosion occurring at the defect under disbonded coating.

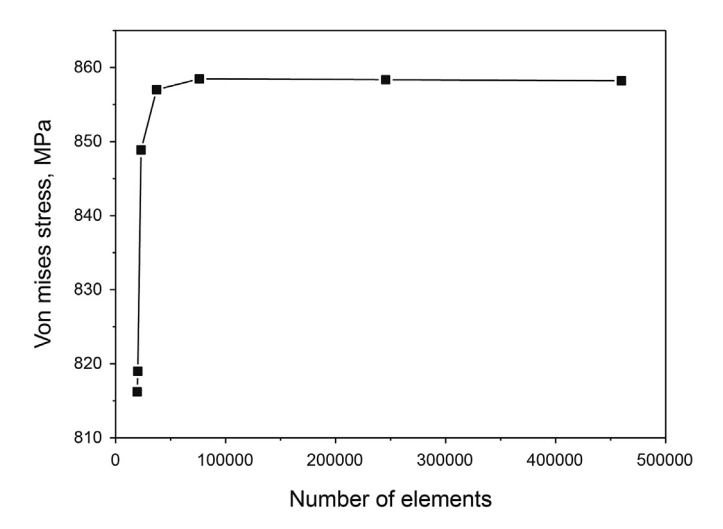


Fig. 3. Maximum von Mises stress at the corrosion defect (θ is 0° and internal pressure is 20 MPa) as a function of the number of elements.

deoxygenated NS4 solution, electrochemical reactions of steel are expressed as (Park et al., 2002):

Anodic reaction: Fe
$$\rightarrow$$
 Fe²⁺ + 2e (4)

Cathodic reaction:
$$2H^+ + 2e \rightarrow H_2$$
 (5)

For the cathodic reaction in deoxygenated NS4 solution, the reduction of either hydrogen ions or water is possible, but the reduction of dissolved oxygen is negligible. According to Nernst equation (pH 6.8, temperature 25 °C), the equilibrium potentials for hydrogen ion reduction, i.e., reaction (5) and water reduction (H₂O+ 2e \rightarrow H₂ + 2OH $^-$) are both -0.40 V (standard hydrogen electrode, SHE). Thermodynamically, the reduction reactions of hydrogen ions and water are identical at the given condition. Even the two reactions have different exchange current densities at the equilibrium potential, the values are not directly related to corrosion current density at the steady-state corrosion condition. Thus, the hydrogen ion reduction as the cathodic reaction in this work is mainly based on thermodynamic consideration.

The electrochemical reaction kinetics are under activation-controlled, where anodic/cathodic current densities (i_a/i_c) are written as (Liu et al., 2009):

$$i_{a} = i_{0,a} \exp\left(\frac{\varphi_{a} - \varphi_{a,eq}}{b_{a}}\right) \tag{6}$$

$$i_{c} = i_{0,c} \exp\left(\frac{\varphi_{c} - \varphi_{c,eq}}{b_{c}}\right) \tag{7}$$

where $i_{0,a}/i_{0,c}$, φ_a/φ_c , $\varphi_{a,eq}/\varphi_{c,eq}$ and b_a/b_c are anodic/cathodic exchange current densities, electrode potentials, equilibrium electrode potentials and Tafel slopes, respectively. According to published work (Xu and Cheng, 2013), $i_{0,a}$ and $i_{0,c}$ for reactions (4) and (5), were calculated from the potentiodynamic polarization curve, and the values are 2.353×10^{-7} A/cm² and 1.457×10^{-6} A/cm², respectively. The cathodic exchange current density meets the value for hydrogen ion reduction. The values of b_a and b_c are 0.118 V/decade and -0.207 V/decade, respectively. The electrochemical corrosion parameters depend on both pipeline steel and corrosive environment. In other words, these parameters should be measured in specific corrosion systems and a model is then developed based on the input parameters. Based on Nernst

equation, $\varphi_{a,eq}$ and $\varphi_{c,eq}$ can be calculated as:

$$\varphi_{a,eq} = \varphi_{a,eq}^{0} + \frac{RT}{2F} \ln(a_{Fe^{2+}})$$
(8)

$$\varphi_{c,eq} = \varphi_{c,eq}^0 + \frac{RT}{F} \ln(a_{H^+})$$
(9)

where $\varphi_{\rm a,eq}^0$ and $\varphi_{\rm c,eq}^0$ are anodic and cathodic standard equilibrium potentials for reactions (4) and (5), which are -0.44 V (standard hydrogen electrode, SHE) and 0 V (SHE), respectively (Bagotsky, 2006), R is ideal gas constant of 8.314 J/K·mol, T is thermodynamic temperature of 298.15 K, and F is Faraday's constant of 96485.34 C/mol. Reference (Xu and Cheng, 2013) gives the ferrous ion activity, $a_{\rm Fe^{2+}}$, of 10^{-6} M and the hydrogen ion activity, $a_{\rm H^+}$, of $10^{-6.8}$ M (pH 6.8 in NS4 solution). Thus, $\varphi_{\rm a,eq}$ and $\varphi_{\rm c,eq}$ are calculated to be -0.617 V (SHE) and -0.402 V (SHE), respectively.

2.2. Modeling of the M-E effect at corrosion defect

Based on Gutman's theory (Gutman, 1998), the effect of elastoplastic deformation on anodic equilibrium potential is:

$$\varphi_{\mathsf{a},\mathsf{eq}} = \varphi_{\mathsf{a},\mathsf{eq}}^0 + \Delta \varphi_{\mathsf{a},\mathsf{eq}}^\mathsf{e} + \Delta \varphi_{\mathsf{a},\mathsf{eq}}^\mathsf{p} \tag{10}$$

where $\Delta \varphi_{a,eq}^{e}$ and $\Delta \varphi_{a,eq}^{p}$ are shifts of $\varphi_{a,eq}^{0}$ in elastic and plastic deformation regions, respectively, which can be written as:

$$\Delta \varphi_{\rm a,eq}^{\rm e} = -\frac{\Delta P V_{\rm m}}{nF} \tag{11}$$

$$\Delta \varphi_{\rm a,eq}^{\rm p} = -\frac{TR}{nF} \ln \left(\frac{v\alpha}{N_0} \varepsilon_{\rm pe} + 1 \right) \tag{12}$$

where ΔP is the excess pressure which is about 1/3 of $\sigma_{\rm Mises}$ in elastic strain region or 1/3 of yield stress ($\sigma_{\rm ys}$) of the steel in plastic strain region, $V_{\rm m}$ is molar volume (7.13 \times 10⁻⁶ m³/mol), n is number of charge (2), ν is an orientation-dependent factor (0.45), α is a coefficient (1.67 \times 10¹¹cm⁻²), N_0 is the initial density of dislocations prior to plastic deformation (1 \times 10⁸ cm⁻²) (Gutman, 1998), and $\varepsilon_{\rm ep}$ is effective plastic strain from mechanical elasto-plastic simulation.

In the FE modeling, the hardening function σ_h (ε_{ep}) was used to describe the plastic deformation of the steel, thus the σ_{ys} is modified as (Liu et al., 2009; Xu and Cheng, 2012c):

$$\sigma_{\rm ys} = \sigma_{\rm ys0} + \sigma_{\rm h}(\varepsilon_{\rm pe}) \tag{13}$$

where σ_{ys0} is initial yield stress of steels, and σ_h is derived from the experimental stress function according to the true stress-strain curve in the plastic train region. The yield stress, the ultimate tensile strength and Young's modulus of $\times 100$ pipeline steel are 806 MPa, 891 MPa and 207 GPa, respectively (Xu and Cheng 2012a, 2017).

The cathodic reaction is also accelerated by the M-E interaction, and $i_{0,c}$ is described using a semi-empirical expression as (Xu and Cheng, 2013):

$$i'_{0,c} = i_{0,c} \times 10^{\frac{\sigma_{\text{Mises}} V_{\text{m}}}{6F(-b_c)}}$$
 (14)

3. Results and discussion

3.1. Validation of the FE simulation results

The corrosion potential and net current density (i.e., $i_{net} = i_a + i_c$) of ×100 pipeline steel in NS4 solution obtained from the modeling and experimental testing in authors' previous work (Shuai et al., 2017: Sun and Cheng. 2018: Wang et al., 2018: Xu and Cheng 2013, 2017, 2017; Fatoba et al., 2018; Wang and Han, 2013) are shown in Fig. 4, where a microprobe technique was used to measure E_{corr} , i_a and i_c on a steel specimen uniaxially stressed at various level. To ensure the modeling results comparable with the experimental data, the initial and boundary conditions are set identical to those in experimental testing, including solution chemistry, pH, steel grade ($\times 100$ steel) and the properties, etc. Generally, the corrosion potential decreases slightly in the elastic region. When σ_{Mises} exceeds 806 MPa, the corrosion potential drops rapidly to the negative direction in the plastic region. Similar changes are observed on i_{net} that is approximately equal to zero in the elastic region, indicating the balanced anodic and cathodic reaction. However, the i_{net} increases significantly towards the anodic direction when the plastic deformation presents, indicating that the stress enhanced corrosion under the M-E effect during plastic deformation. Besides, the difference between modeling results and the experimental data is slight, indicating a good accuracy of the FE simulation of the M-E interaction. It is noted that many factors can affect the modeling results. Moreover, experimental tests can be manually controlled to obtain matching results with the modeling. Therefore, more tests are required to provide sufficient data to support the reliability of modeling.

3.2. Distributions of σ_{Mises} and E_{corr} at defect with varied orientations on the pipe

To assess the effect of the defect orientation on the local M-E effect, the semi-ellipsoidal defect is taken with the values of a (half-

length of the secondary axis of corrosion defect), b (depth of corrosion defect) and c (half-length of the primary axis) of 8 mm, 8 mm and 32 mm, respectively. The distribution of $\sigma_{\rm Mises}$ at the defect with varied θ degrees (the inclination of the defect between its primary axis and the longitudinal direction of the pipe) is shown in Fig. 5, under 20 MPa of internal pressure. When θ is 0° or 90°, respectively, the dark red and red colors are observed at the defect center and the blue color at both sides of the defect, indicating that a stress concentration occurs at the center and the tips of the defect, while the sides of the defect are under low stress. With the θ changing from 0° to 90°, the stress concentration level reduces according to color changing from dark red to light red. Moreover, when θ is not equal to 0° or 90°, the stress distribution is not symmetric, and the most asymmetrical stress distribution occurs at θ of 45°.

Fig. 6 indicates that the distribution of E_{corr} at the defect with varied θ degrees under 20 MPa internal pressure. With the θ changing from 0° to 90° , $E_{\rm corr}$ is shifted less negatively, as shown through the color change from dark red to dark blue. When θ is 0° , the dark red color at the defect center than both sides of the defect shows the most negative $E_{\rm corr}$ at the center. As the θ is equal to 90°, the entire defect is uniformly colored with dark blue, indicating the uniform distribution of corrosion potential. When θ is 0° or 90° , the symmetry of E_{corr} distribution does not exist, where the most asymmetrical distribution of $E_{\rm corr}$ is also observed at θ of 45°. In the comparison of the stress and corrosion potential distributions ate the corrosion defect in Figs. 5 and 6, the defect site with a high stress concentration level is always associated with a negative corrosion potential. The negative corrosion potential of a steel indicates a great corrosion activity in aqueous solutions, thus the stress concentration would enhance the corrosion at the defect.

The distributions of $\sigma_{\rm Mises}$ at the defect and the potential field in the solution with varied θ is shown in Fig. 7, where the left graph is cross-section perpendicular to z-axis (i.e., the longitudinal direction) and the right is the cross-section perpendicular to x-axis (i.e., the circumferential direction). It is seen that, for the left graph, as θ

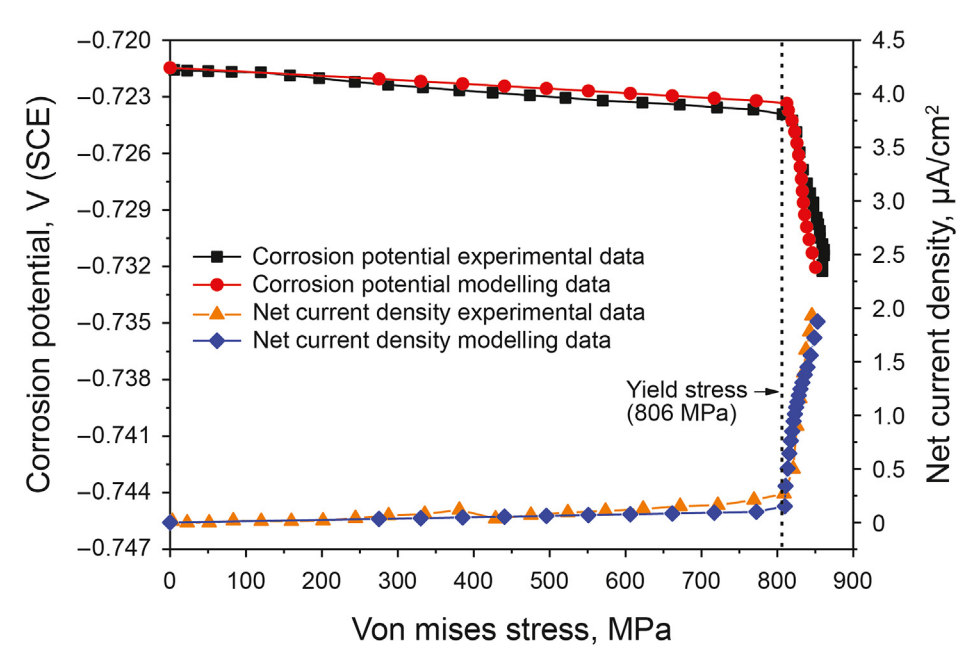


Fig. 4. Corrosion potential and net current density of X100 pipeline steel in NS4 solution as a function of von Mises stress obtained from the modelling and experimental testing in authors' previous work (Xu and Cheng, 2013).

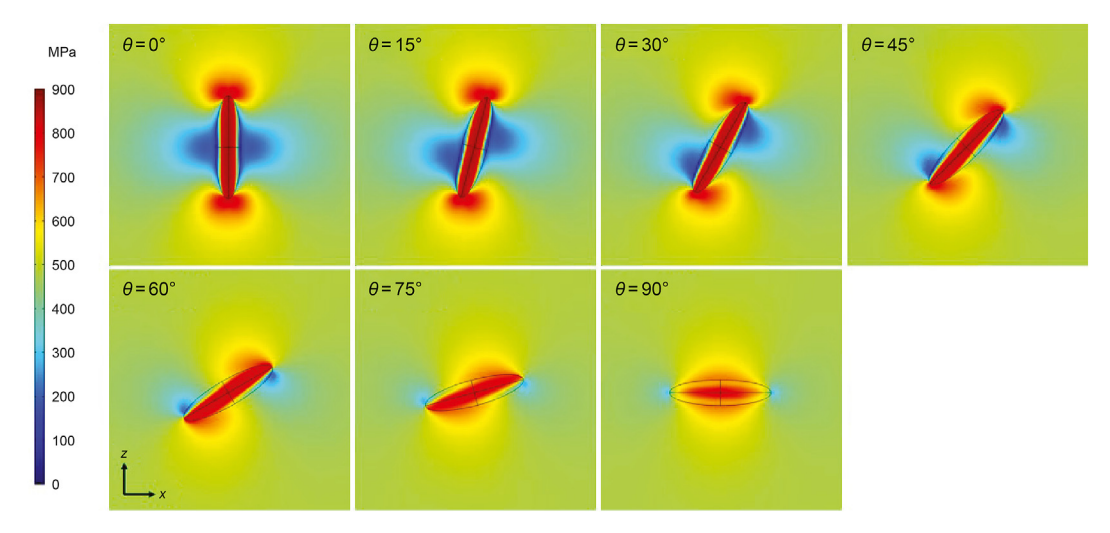


Fig. 5. Distribution of von Mises stress at the corrosion defect with varied θ angles, which indicate the inclination of the defect between its primartily axis and the longitudinal direction of the pipe, under 20 MPa of internal pressure.

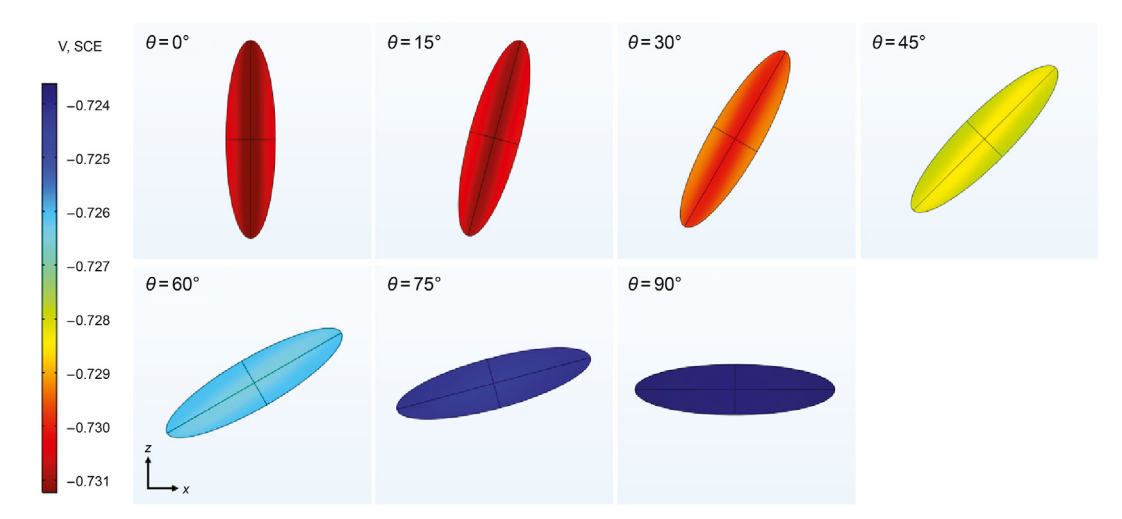


Fig. 6. Distribution of corrosion potential at the defect with varied θ angles under 20 MPa of internal pressure.

changes from 0° to 90° , the circumferential length of the defect along the *x*-axis increases from 2a (16 mm) to 2c (64 mm), the stress concentration zone (red color region) becomes small. However, for the right graph, as θ changes from 0° to 90° , the longitudinal length of the defect along the *z*-axis decreases from 2c to 2a, which also accompanies with the reduced high stress zone at the defect. At the same time, the solution potential changes as the potential of the corrosion defect changes. The electric field in the solution phase is dependent on local potential at the defect. The greater level of stress concentration, the more negative potential of the defect, which is consistent with the color of the solution phase changing from dark red to dark blue.

The reason that stress distribution is influenced by the θ is the difference between σ_H and σ_L of the pipe resulted from P. According to Eq. (3), σ_H is about three times of σ_L . Thus, the effect of σ_H on local stress concentration is greater than σ_L . For a defect with varied θ on the pipe, when the length of the defect in the z-axis direction that is perpendicular to σ_H is longer, the local stress at the defect is higher. This particularly applies for the defect with θ of 0°. As the θ changes from 0° to 90°, the primary length of the defect in the z-axis direction becomes shorter, and the local stress concentration level reduces.

3.3. Distributions of σ_{Mises} , E_{corr} , i_a and i_c across the defect with varied orientations on the pipe

Fig. 8 indicates that the distribution of $\sigma_{\rm Mises}$ along the defect in the z-axis (i.e., longitudinal) direction with varied θ degrees under 20 MPa internal pressure. The maximum $\sigma_{\rm Mises}$ at the defect with all inclination angles exceed 806 MPa under 20 MPa internal pressure. However, the greatest stress concentration level can be observed when θ is 0°, and the stress over the whole defect is more than the yield stress of the steel. When θ changes from 0° to 90°, the maximum $\sigma_{\rm Mises}$ reduces from 856.61 MPa to 808.22 MPa. At θ of 90°, only a small section of the defect center has the stress concentration level exceeding the yield stress, while the stress of the majority segment of the defect is below the yield level (see Fig. 8).

Fig. 9 indicates that the distribution of $E_{\rm corr}$ along the z-axis (i.e., longitudinal) direction of the defect with varied θ degrees under 20 MPa internal pressure. $E_{\rm corr}$ of the defect is the most negative when θ is equal to 0°. With the θ increasing from 0° to 90°, $E_{\rm corr}$ is shifted less negatively. Besides, the greater stress concentration level means a more negative shift of $E_{\rm corr}$, which would increase the steel corrosion. Generally, $E_{\rm corr}$ distribution at the defect is almost uniform at all angles. This is because the effect of elastic

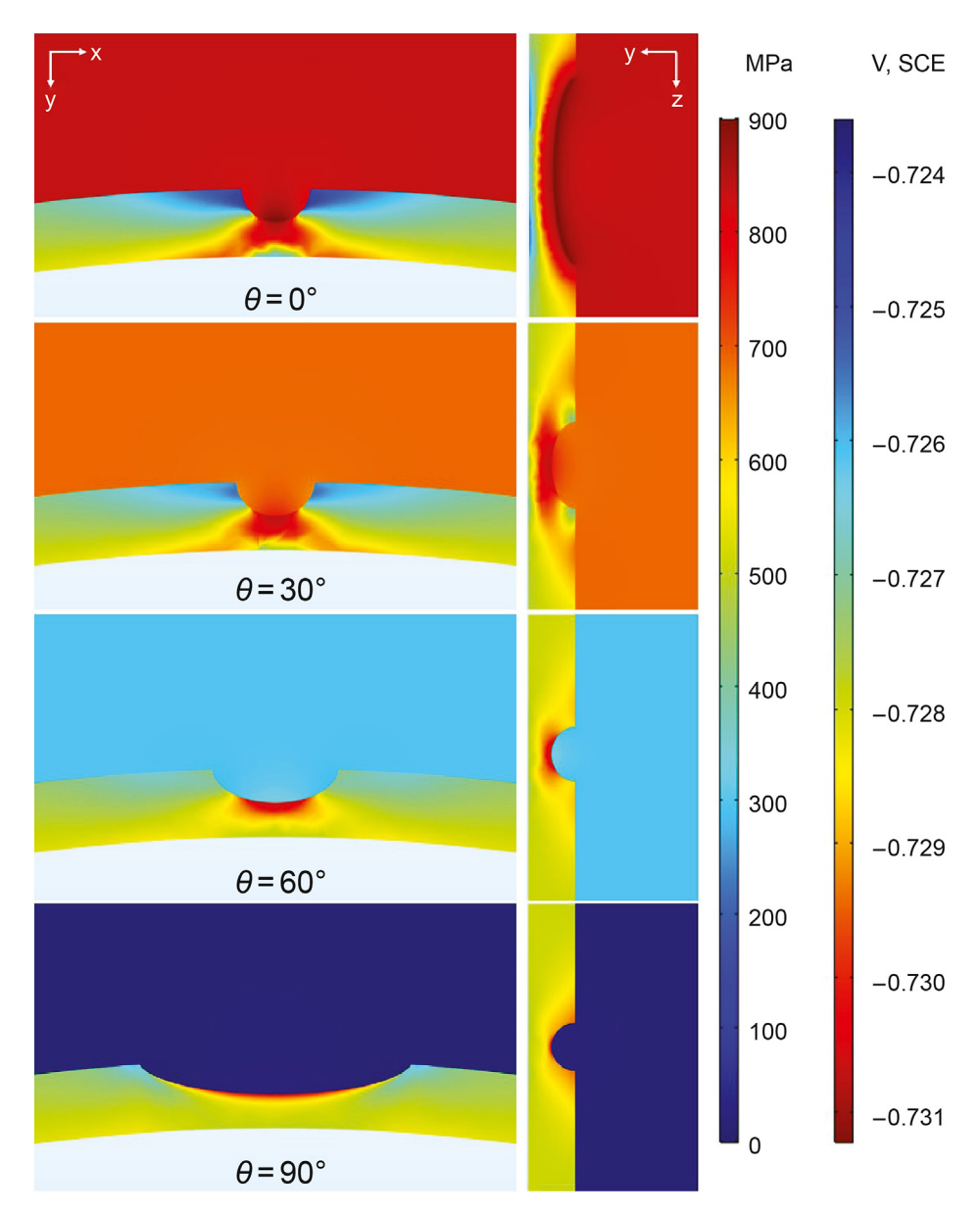


Fig. 7. Distributions of von Mises stress at the defect and the potential field in the solution with varied θ angles, where the left graph is the cross section perpendicular to z-axis (i.e., the longitudinal direction) and the right is the cross section perpendicular to x-axis (i.e., the circumferential direction).

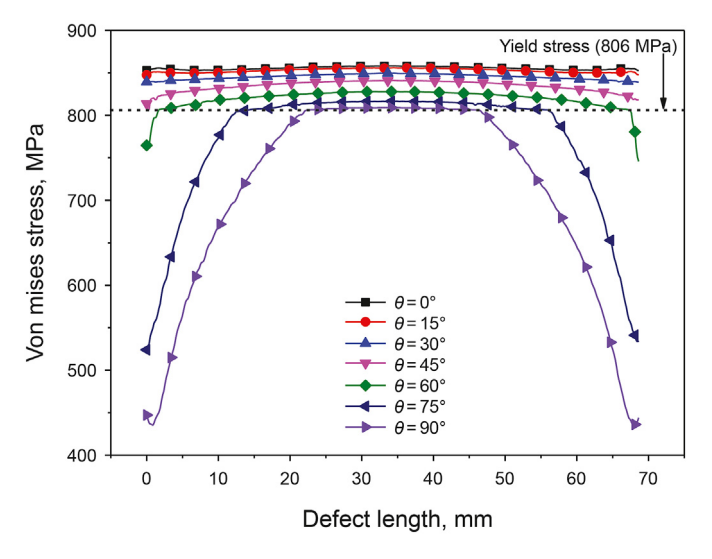
deformation on E_{corr} is negligible although the stress change in the elastic region is large. Moreover, the change of the plastic strain is small in the primary axis direction of the defect, as seen in Fig. 8.

The distributions of i_a and i_c along the z-axis (i.e., longitudinal) direction of the defect with varied θ degrees under 20 MPa of internal pressure are shown in Fig. 10. The absolute values of both i_a and i_c are the greatest when θ is equal to 0°. With the θ changing from 0° to 90°, i_a and i_c decrease. The results show that the M-E interaction accelerates the anodic and cathodic dissolution rate of the corrosion defect together. Furthermore, the difference of i_a between the center of the defect and its sides reaches the maximum at the θ of 45°, indicating the greatest non-uniformity of the anodic reaction rates at this inclination angle. The reason is that the difference between the plastic strain at the center of the defect and its sides is the greatest at the θ of 45°.

3.4. σ_{Mises} , E_{corr} , i_a and i_c at the center of the defect with varied orientations on the pipe under various internal pressures

The variation of σ_{Mises} at the defect center (i.e., the maximum σ_{Mises}) under various internal pressures (P) with the change of inclination angle θ is shown in Fig. 11. As the angle θ changes from 0° to 90°, the maximum σ_{Mises} decreases. This is particularly obvious at low P such as 5 MPa. When P is 5 MPa, the maximum σ_{Mises} of the defect is lower than the yield stress and the defect is in the elastic region. When P increases to 10 MPa and 15 MPa, the maximum σ_{Mises} exceeds the yield stress at small θ angles. When P is up to 20 MPa, the maximum σ_{Mises} at all θ degrees are greater than the yield stress and the defect is in the plastic region.

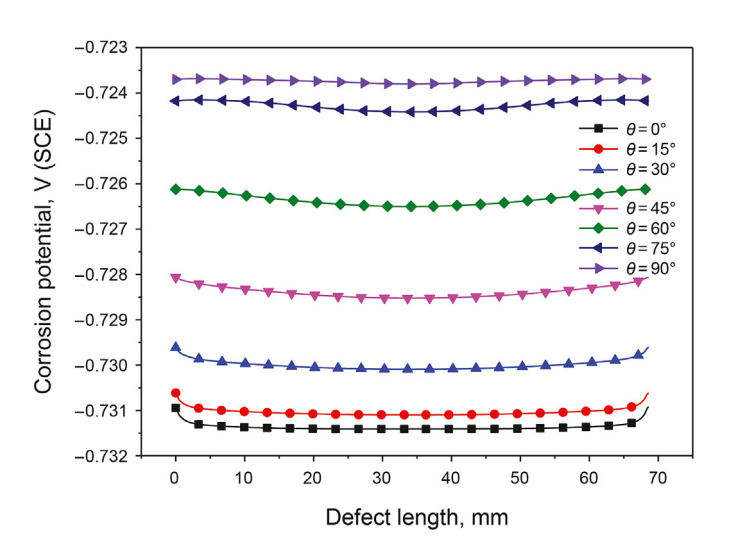
The variation of E_{corr} at the defect center under various P with the change of inclination angle θ is shown in Fig. 12. At specific P,



Von mises stress, MPa 20 MPa 15 MPa 10 MPa 5 MPa θ,

Fig. 8. Distribution of von Mises stress along the z-axis (i.e., longitudinal) direction of the defect with varied θ angles under 20 MPa of internal pressure.

Fig. 11. The variation of von Mises stress at the defect center under varied internal pressures with the change of inclination angle θ .



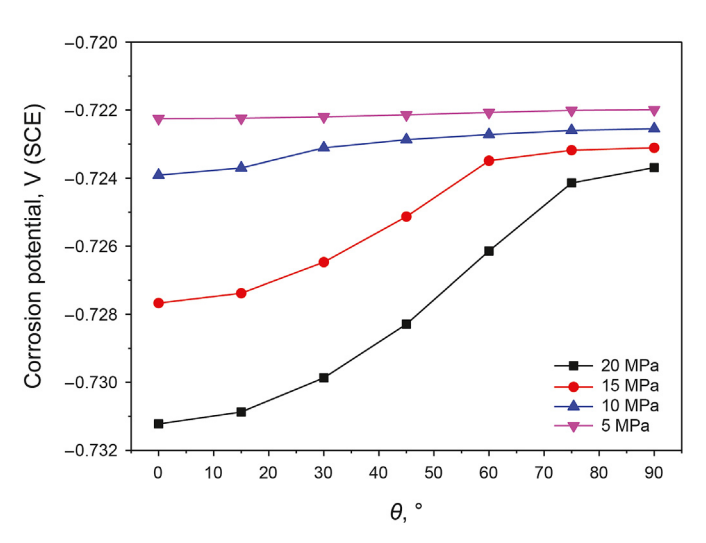


Fig. 9. Distribution of corrosion potential along the z-axis (i.e., longitudinal) direction of the defect with varied θ angles under 20 MPa of internal pressure.

Fig. 12. The variation of corrosion potential at the defect center under varied internal pressures with the change of inclination angle θ .

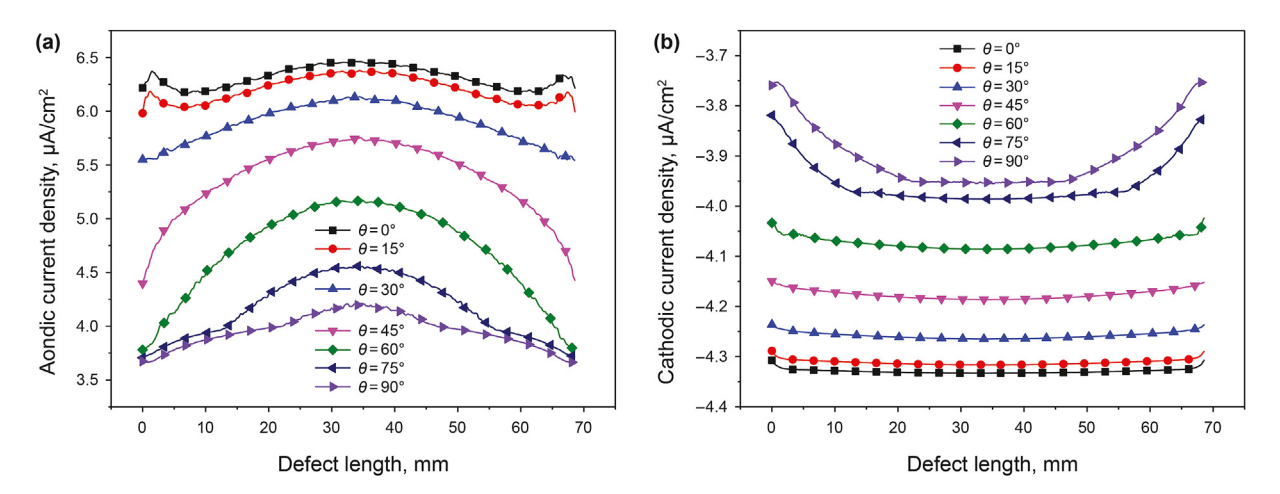


Fig. 10. Distributions of (a) anodic and (b) cathodic current densities along c-axis direction of the defect with varied θ angles under 20 MPa of internal pressure.

with the θ changing from 0° to 90°, $E_{\rm corr}$ is shifted less negatively. While the change of $E_{\rm corr}$ is remarkable with the θ angle at high P such as 20 MPa, there is little change of $E_{\rm corr}$ at low internal pressures such as 5 MPa. At a fixed defect inclination angle, the $E_{\rm corr}$ becomes more negative as the internal pressure increases.

The variations of i_a and i_c at the defect center under various P with the change of inclination angle θ are shown in Fig. 13. At specific P, with the θ changing from 0° to 90° , both i_a and i_c at the defect center decrease (note the absolute value of cathodic current density). As P increases while the θ angle is fixed, i_a and i_c also increase. The results show that an elevated P of the pipe would accelerate both anodic and cathodic reactions at the defect center, where the corrosion rate is enhanced. Moreover, the defect with θ of 0° is always associated with increased corrosion (i.e., increased i_a). Although the difference in corrosion potential caused by the change of the defect inclination (θ) is small (Fig. 6), the anodic and cathodic current densities change apparently with θ . Potential is a thermodynamic parameter and current density is a kinetic parameter. It is not uncommon that a small change in thermodynamic parameter (e.g., corrosion potential) can cause a big change in reaction kinetics. Thus, the corrosion rate at the defect can be affected by the defect inclination on pipelines.

3.5. Effect of the defect geometry (i.e., the r_{ca} ratio) on σ_{Mises} , E_{corr} , i_a and i_c of the defect

The defect geometry is defined using the $r_{\rm ca}$ ratio, but the defect depth is maintained unchanged. Since c is longer than the secondary axis (a) for a semi-ellipsoidal defect, the stress distribution and local corrosion condition at the defect would be affected by the inclination angle θ .

The variation of $\sigma_{\rm Mises}$ at the center of the defect with θ of 0° and 90° under 20 MPa of internal pressure with the change of $r_{\rm ca}$ ratio is shown in Fig. 14. When the defect shape is semi-sphere ($r_{\rm ca}=1$), the effect of θ on the maximum $\sigma_{\rm Mises}$ can be negligible. With the increase of $r_{\rm ca}$, i.e., the length of c increases or the length of a becomes short, the role of the inclination angle in the stress at the defect is more obvious, where the stress at θ of 0° increases much more rapidly than that at θ of 90° . When $r_{\rm ca}$ is 8, the maximum $\sigma_{\rm Mises}$ of the defect with θ of 0° reaches 892.13 MPa and exceeds the ultimate tensile stress of the steel. Thus, the corrosion defect with the c-axis much longer than a-axis is really weaker sites on pipelines in terms of the stress concentration development.

The variation of $E_{\rm corr}$ at the center of the defect with θ of 0° and 90° under 20 MPa of internal pressure with the change of $r_{\rm ca}$ ratio is

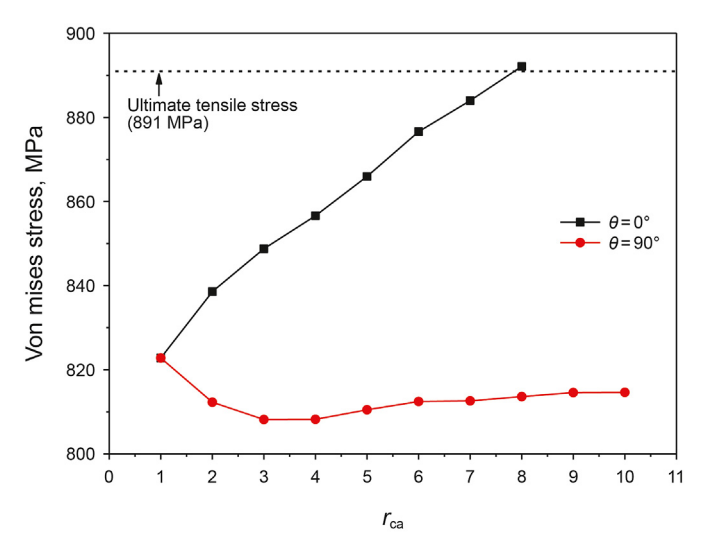


Fig. 14. The variation of von Mise stress at the center of the defect (with θ of 0° and 90°) under 20 MPa internal pressure with the change of rea ratio.

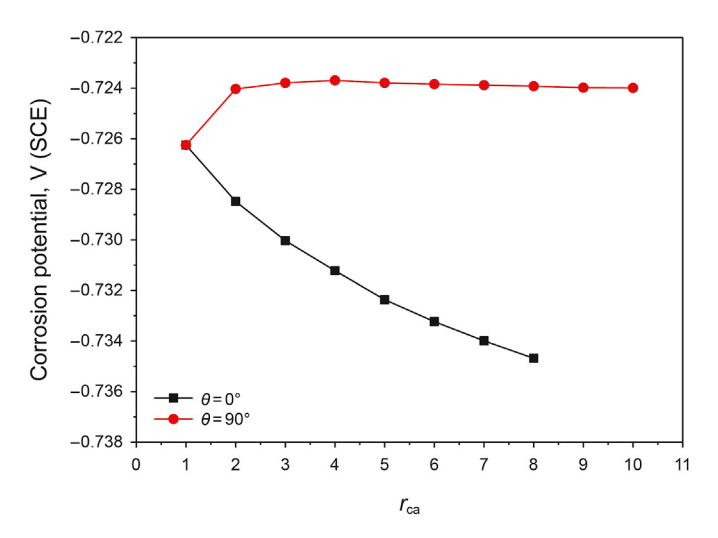


Fig. 15. The variation of corrosion potential at the center of the defect (with θ of 0° and 90°) under 20 MPa internal pressure with the change of rca ratio.

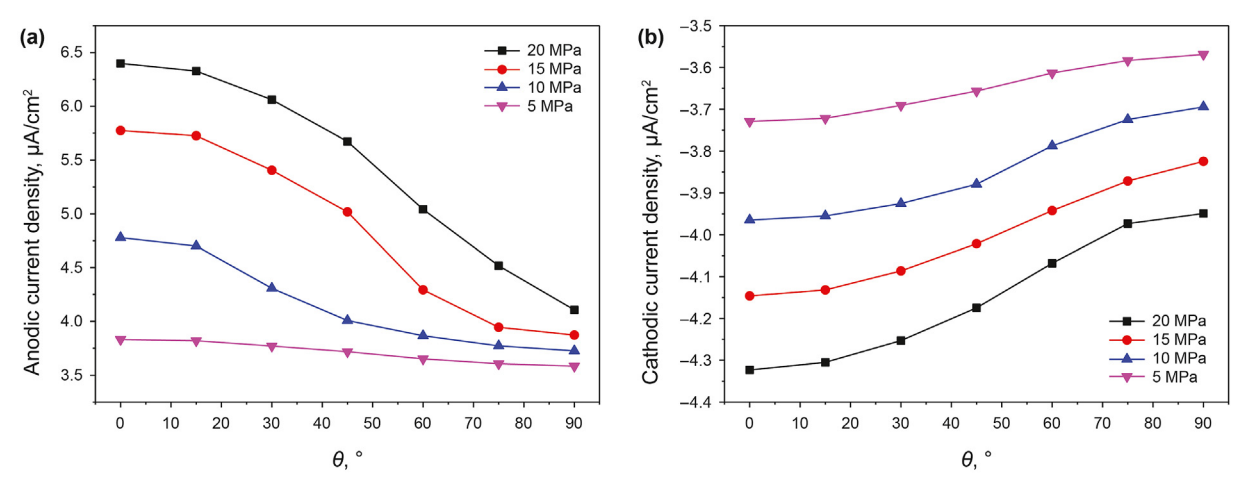


Fig. 13. The variations of (a) anodic and (b) cathodic current densities at the defect center under varied internal pressures with the change of inclination angle θ .

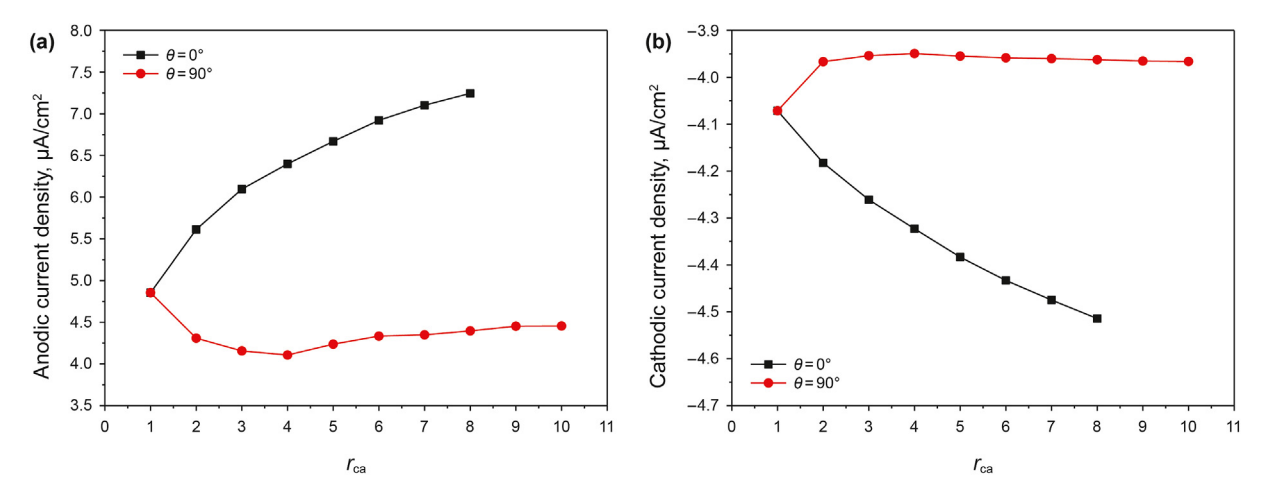


Fig. 16. The variations of (a) anodic and (b) cathodic current densities at the center of the defect (with θ of 0° and 90°) under 20 MPa internal pressure with the change of rca ratio.

shown in Fig. 15. The change of $E_{\rm corr}$ with the increase in $r_{\rm ca}$ ratio is similar to previous results. When $r_{\rm ca}=1$, $E_{\rm corr}$ of the defect is equal for θ of 0° and 90° . As the $r_{\rm ca}$ ratio increases, the corrosion potential of the defect at θ of 0° shifts negatively, while that at θ of 90° goes towards the less negative direction slightly. Since the negative $E_{\rm corr}$ is accompanied with a great corrosion reaction, the defect with θ of 0° becomes more corrosion-active, which is accompanied with the rapidly increased stress concentration level (Fig. 14).

The variations of i_a and i_c at the center of the defect with θ of 0° and 90° under 20 MPa of internal pressure with the change of $r_{\rm ca}$ ratio is shown in Fig. 16. When $r_{\rm ca}=1$, i_a and i_c of the defect are identical for the θ angles of 0° and 90° . With the increase of the ratio $r_{\rm ca}$, and the absolute values of i_a and i_c increase on the defect with θ of 0° , indicating the accelerated corrosion reactions, as compared with the defect with θ of 90° . Thus, in terms of the long-term corrosion defect growth, the defect with the inclination angle of 0° tends to develop accelerated localized corrosion, causing the pipeline failure.

4 Conclusions

The M-E interaction at a defect on pipelines is extremely affected by the defect orientation, i.e., the inclination angle (θ) . Since the hoop stress is about three times of the longitudinal stress of the pipe under internal pressure, the stress concentration occurring at the defect is not uniform when it is inclined to the pipe longitudinal direction with a θ . Generally, the stress is greater in the x-axis direction than that in the z-axis direction.

When the inclination angle is zero, the greatest stress concentration level at the defect can be observed, which is associated with the most negative $E_{\rm corr}$ and the greatest $i_{\rm a}$. The corrosion defect with the primary axis parallel to the longitudinal direction of the pipe ($\theta=0^{\circ}$) can experience accelerated localized corrosion. With θ increasing from 0° to 90° , the stress concentration level reduces and $E_{\rm corr}$ becomes less negative, accompanying with a decreased $i_{\rm a}$. The dependence of the stress concentration level and M-E effect on the θ is more apparent at elevated internal pressures.

When the ratio $r_{\rm ca}$ of corrosion defect is equal to 1, the defect inclination does not affect $\sigma_{\rm Mises}$, $E_{\rm corr}$, $i_{\rm a}$ and $i_{\rm c}$ at the defect. With the increase of $r_{\rm ca}$ (i.e., the primary axial length c exceeds the secondary axial length a), the effect of inclination angle (θ) is more apparent. $\sigma_{\rm Mises}$, $E_{\rm corr}$, $i_{\rm a}$ and $i_{\rm c}$ at the defect with a θ of 0° change remarkably, while there is little change for the defect with θ of 90°.

Acknowledgements

This work was supported by the National Natural Science Foundation of China (No. 51705077), Natural Science Foundation of Fujian Province (No.2018J01768), and the University of Calgary.

References

ASME B31.4, 2009. Pipeline Transportation Systems for Liquid Hydrocarbons and Other Liquids. The American Society of Mechanical Engineers.

Bagotsky, V.S., 2006. Fundamentals of Electrochemistry, second ed. John Wiley & Sons, Inc.

Chouchaoui, B.A., Pick, R.J., 1996. Behaviour of longitudinally aligned corrosion pits. Int. J. Pres. Ves. Pip. 67, 17–35. https://doi.org/10.1016/0308-0161(94)00057-3.

Dai, M.J., Liu, J., Huang, F., Zhang, Y.H., Cheng, Y.F., 2018. Effect of cathodic protection potential fluctuations on pitting corrosion of X100 pipeline steel in acidic soil environment. Corrosion Sci. 143, 428–437. https://doi.org/10.1016/ j.corsci.2018.08.040.

Fatoba, O.O., Leiva-Garcia, R., Lishchuk, S.V., Larrosa, N.O., Akid, R., 2018. Simulation of stress-assisted localised corrosion using a cellular automaton finite element approach. Corrosion Sci. 137, 83—97. https://doi.org/10.1016/j.corsci.2018.03.029.

Gutman, E.M., 1998. Mechanochemistry of Materials. Cambridge Interscience Publishing.

Huang, Y.F., Wei, C., Chen, L.J., Li, P.F., 2014. Quantitative correlation between geometric parameters and stress concentration of corrosion pits. Eng. Fail. Anal. 44, 168–178. https://doi.org/10.1016/i.engfailanal.2014.05.020.

Kim, Y., Park, K.J., 2017. Characterization of axial and oblique defects in pipes using fundamental torsional guided modes. NDT Int. 92, 149–158. https://doi.org/ 10.1016/j.ndteint.2017.08.006.

Liu, B., Liu, X.J., Zhang, H., 2009. Strain-based design criteria of pipelines. J. Loss Prev. Process. Ind. 22, 884–888. https://doi.org/10.1016/j.jlp.2009.07.010.

Liu, H.W., Cheng, Y.F., 2017. Mechanism of microbiologically influenced corrosion of X52 pipeline steel in a wet soil containing sulfate-reduced bacteria. Electrochim. Acta 253, 368–378. https://doi.org/10.1016/j.electacta.2017.09.089.

Liu, H.W., Cheng, Y.F., 2018. Mechanistic aspects of microbially influenced corrosion of X52 pipeline steel in a thin layer of soil solution containing sulphatereducing bacteria under various gassing conditions. Corrosion Sci. 133, 178–189. https://doi.org/10.1016/j.corsci.2018.01.029.

Lu, Y.X., Jing, H.Y., Han, Y.D., Xu, L.Y., 2018. A finite element model of carbon steel welded joint corrosion under plastic strain. Mater. Corros. 69, 227–238. https:// doi.org/10.1002/maco.201709620.

Noda, N.A., Hayashida, H., 2000. Interaction between elliptical and ellipsoidal inclusions under bending stress fields. Arch. Appl. Mech. 70, 612–624. https://doi.org/10.1007/s004190000093

Park, J.J., Pyun, S.I., Na, K.H., Lee, S.M., Kho, Y.T., 2002. Effect of passivity of the oxide film on low-pH stress corrosion cracking of API 5L X-65 pipeline steel in bicarbonate solution. Corrosion 58, 329–336. https://doi.org/10.5006/1.3287682.

Qian, S., Cheng, Y.F., 2017. Accelerated corrosion of pipeline steel and reduced cathodic protection effectiveness under direct current interference. Construct. Build. Mater. 148, 675–685. https://doi.org/10.1016/j.conbuildmat.2017.05.024.

Rajabipour, A., Melchers, R.E., 2013. A numerical study of damage caused by combined pitting corrosion and axial stress in steel pipes. Corrosion Sci. 76, 292–301. https://doi.org/10.1016/j.corsci.2013.07.002.

Shuai, Y., Shuai, J., Xu, K., 2017. Probabilistic analysis of corroded pipelines based on a new failure pressure model. J Eng Fail Anal 81, 216–233. https://doi.org/

10.1016/j.engfailanal.2017.06.050.

- Sun, J.L., Cheng, Y.F., 2018. Assessment by finite element modeling of the interaction of multiple corrosion defects and the effect on failure pressure of corroded pipelines. Eng. Struct. 65, 278–286. https://doi.org/10.1016/j.engstruct.2018.03.040.
- Sun, J.L., Cheng, Y.F., 2019. Investigation by numerical modeling of the mechanoelectrochemical interaction of circumferentially aligned corrosion defects on pipelines. Thin-Walled Struct. 144, 106314. https://doi.org/10.1016/ i.tws.2019.106314.
- Wang, H.K., Yang, Y., Yu, J.X., Duan, J.H., Wang, Cm, 2018. Effect of 3D random pitting defects on the collapse pressure of pipe Part I: Experiment. Thin-Walled Struct. 129, 512–526. https://doi.org/10.1016/j.tws.2018.04.015.
- Wang, H.T., Han, E.H., 2013. Simulation of metastable corrosion pit development under mechanical stress. Electrochim. Acta 90, 128–134. https://doi.org/ 10.1016/j.electacta.2012.11.056.
- Xie, M.J., Tian, Z.G., 2018. A review on pipeline integrity management utilizing inline inspection data. Eng. Fail. Anal. 92, 222–239. https://doi.org/10.1016/ j.engfailanal.2018.05.010.
- Xu, L.Y., Cheng, Y.F., 2012a. Corrosion of X100 pipeline steel under plastic strain in a neutral pH bicarbonate solution. Corrosion Sci. 64, 145–152. https://doi.org/ 10.1016/j.corsci.2012.07.012.
- Xu, L.Y., Cheng, Y.F., 2012b. An experimental investigation of corrosion of X100 pipeline steel under uniaxial elastic stress in a near-neutral pH solution.

- Corrosion Sci. 59, 103-111. https://doi.org/10.1016/j.corsci.2012.02.022.
- Xu, L.Y., Cheng, Y.F., 2012c. Reliability and failure pressure prediction of various grades of pipeline steel in the presence of corrosion defects and pre-strain. Int. J. Pres. Ves. Pip. 89, 75–84. https://doi.org/10.1016/j.ijpvp.2011.09.008.
- Xu, L.Y., Cheng, Y.F., 2013. Development of a finite element model for simulation and prediction of mechanoelectrochemical effect of pipeline corrosion. Corrosion Sci. 73, 150–160. https://doi.org/10.1016/j.corsci.2013.04.004.
- Xu, L.Y., Cheng, Y.F., 2017. A finite element based model for prediction of corrosion defect growth on pipelines. Int. J. Pres. Ves. Pip. 153, 70–79. https://doi.org/ 10.1016/j.ijpvp.2017.05.002.
- Xu, L.Y., Su, X., Cheng, Y.F., 2013. Effect of alternating current on cathodic protection on pipelines. Corrosion Sci. 66, 263–268. https://doi.org/10.1016/ j.corsci.2012.09.028.
- Yajima, A., Wang, H., Liang, R.Y., Castaneda, H., 2015. A clustering based method to evaluate soil corrosivity for pipeline external integrity management. Int. J. Pres. Ves. Pip. 126, 37–47. https://doi.org/10.1016/j.ijpvp.2014.12.004.
- Yi, D., Idapalapati, S., Xiao, Z.M., Kumar, S.B., 2012. Fracture capacity of girth welded pipelines with 3D surface cracks subjected to biaxial loading conditions. Int. J. Pres. Ves. Pip. 92, 115–126. https://doi.org/10.1016/j.ijpvp.2011.10.019.
- Zhang, Z.W., Ni, X., Cheng, Y.F., 2020. Assessment by finite element modelling of the mechano-electrochemical interaction at double-ellipsoidal corrosion defect with varied inclinations on pipelines. Construct. Build. Mater. 260, 120459. https://doi.org/10.1016/j.conbuildmat.2020.120459.